Reaction Rate Modeling in Noncatalytic Gas–Solid Systems: Species Transport and Mechanical Stress

Hilmar Rode, Dariusz Orlicki, and Vladimir Hlavacek
Lab. for Ceramic and Reaction Engineering, Dept. of Chemical Engineering
State University of New York at Buffalo, Amherst, NY 14260

A detailed model to describe the overall reaction rate of the oxidation of titanium is developed. The mathematical model consists of two facets, the first of which involves a detailed description of species transport that accounts for the formation of charged species. This is augmented by a description of the occurrence of mechanical stress due to a Pilling – Bedworth ratio that differs significantly from 1 as well as differences between precursor and product thermal expansion coefficients. A self-imposed electric field is formed across the oxide layer due to different mobilities of the species considered. This field opposes the transport of electrons and enhances the transport of anion vacancies, thus increasing the overall reaction rate compared to a pure diffusion process, while also ensuring that electrical charge is conserved. Large growth stresses result from the unmatched precursor and product volumes, significantly affecting the overall process. These results show that the incorporation of a consistent treatment of mechanical stress forms a necessary part of any accurate description of the overall behavior of a reacting particle.

Introduction

Determination of the reaction rate of a particle that undergoes a noncatalytic gas–solid reaction is a complex issue that has been extensively studied. In cases where a solid product is formed and the reaction proceeds by means of a defined reaction front, the overall reactivity is governed by the interaction of two major aspects:

1. Chemical reactions and ensuing species transport due to chemical potential differences between the precursor/product and product/gas interfaces.
2. Mechanical stresses that arise due to differences in the precursor and product volumes (Pilling–Bedworth ratio) as well as unmatched thermal expansion coefficients leading to the mechanical degradation of the product layer, thus affecting the overall reactivity.

Several empirical and semiempirical models have been developed for such systems, for example, the shrinking-core model (Levenspiel, 1972), the crackling-core model (Park and Levenspiel, 1975), the grain model (Sohn and Szekely, 1972), the porous pellet model (Ishida and Wen, 1968) and in the field of metal oxidation, the parabolic law (Wagner, 1933) and the logarithmic law (Cabrera and Mott, 1949).

A plateau in the current knowledge base suggests that next-generation modeling efforts are required in order to extend this field of research. Therefore the goal of this work is to develop a detailed model that addresses both the chemical transport and mechanical stress issues in a fundamental and consistent fashion not currently seen in the literature. The oxidation of titanium in an oxygen atmosphere is considered as a case study.

Recently experimental evidence was exhibited on the interaction of transport and stress effects on the overall reactivity of such systems (Rode et al., 1994; Rode, 1994). A detailed model to describe the evolution of mechanical stresses was also developed, assuming that the reaction rate is known. In this study we extend the "coupled currents" approach for the determination of species transport (Rode et al., 1992) on a single particle basis and link it to a detailed stress formulation to yield a model that is consistent and describes the overall reactivity of the gas–solid powder system with a high degree of detail. The stress model has recently been treated in detail (Rode et al., 1994) and is therefore not presented here, although it forms an integral part of the calculation.

Correspondence concerning this article should be addressed to V. Hlavacek.

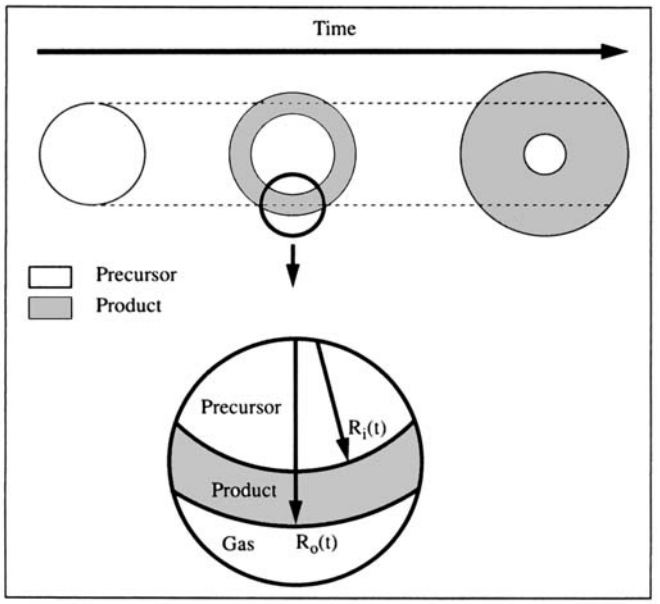

Figure 1. Overall reaction scheme.

Species Transport Model

The oxidation of titanium to titanium dioxide has been chosen as a model system. After an initial product monolayer has formed, either cations or anions have to be transported through the product layer for the further growth of the oxide layer. The mobility of the different species present in the product layer will depend on the defect structure as described by Kubaschewski and Hopkins (1962). If the cation mobility dominates, the product layer will be formed at the product/gas interface, and a hollow core will develop as the overall reaction proceeds. An example of such a case has been given by Colson et al. (1972) for the copper–sulfur system, where SEM micrographs show clearly how the hollow core develops. If the anion mobility dominates, the product layer will be formed at the constrained precursor/product interface, for example, the Ti/TiO_2 system. Under these conditions the reaction scheme will follow the classic "shrinking-core" description.

The overall process is demonstrated in Figure 1, while the microscopic details are shown in Figure 2. The overall reaction consists of several steps, which include the creation and annihilation of charged species at the boundaries and transport of these charged species through the product layer. The

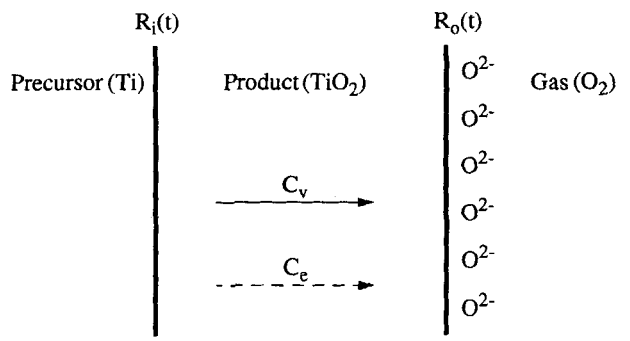

Figure 2. Species transport process.

conversion of precursor takes place at the precursor/product interface $[R_i(t)]$, which is clearly a function of time. However, due to mismatches in the volume of product formed per volume of precursor reacted, the product/gas interface $[R_o(t)]$ is also time dependent. In the case of titanium dioxide the overall particle will tend to swell because the Pilling–Bedworth ratio is larger than 1, as indicated in Figure 1 (Pilling and Bedworth, 1923; Rode et al., 1994). The locations of the two reaction interfaces are given by the solution of the mechanical stress equations. Thus, transport of species and the development of mechanical stresses are intimately coupled and both aspects are solved simultaneously. The stress formulation has been treated in detail (Rode et al., 1994) and only the results are shown in this work—the mathematical equations and numerical methods are not repeated.

TiO_2 is modeled as an n-type oxide with oxygen vacancies as the major defect. This assumption is realistic at relatively high pressure ($> 10^{-5}$ atm) and up to moderate temperatures ($< 1{,}200$°C) as reported by Kofstad (1972) (cf. also Kofstad, 1962; Kofstad, 1967). Reed (1970) reported a homogeneity range for titanium dioxide (TiO_x) of $1.992 < x < 2.000$. It has been shown that at larger deviations from stoichiometry, so-called Magnéli phases that are two phase regions exist (Reed, 1970), as well as lower oxide phases such as TiO, Ti_2O_3, and Ti_3O_5 (Averback et al., 1989; Rode and Hlavacek, 1994). An assumption of this work is that a single phase exists. This is clearly a simplification, as the transport and stress generation will depend on the phases that are formed. This article aims to establish the approach of linking transport (which includes both mass and charge transfer) and stress generation while accounting for the formation of a single phase. The formation of multiple phases is a more realistic case that should be addressed in future work.

The reaction steps used in this model were designed to accommodate the full range of possible behavior that could be exhibited, for example, at relatively high oxygen pressure Ti should be oxidized, while reduction of TiO_2 to Ti should take place at sufficiently low pressure. Various studies that have been conducted on the TiO_2/O_2 interface were used as a source of possible schemes. Göpel et al. (1983) experimentally studied the interaction of the TiO_2 surface with several gases including oxygen. They found that there are two processes present: charge transfer and chemisorption of oxygen molecules, and interaction of oxygen vacancies with chemisorbed species. Munnix and Schmeits (1985) reported that the origin of the surface defects in TiO_2 results from a subsurface oxygen vacancy. Recently, Zhong et al. (1993) performed a comparative study on the local defect structure in vacuum-annealed and hydrogen-annealed rutile by means of scanning tunneling microscopy. These authors found that the defects depended strongly on the method of reduction, but in both cases involved oxygen vacancies. The anion vacancy concentration in TiO_2 can be measured, and depends on oxygen pressure (Buessem and Butler, 1959). These authors also suggested, based on experiment, the oxide/oxygen interface reactions we employ here. Heinrich et al. (1978) conducted an ultraviolet photoemission spectroscopy (UPS) study on the chemisorption of oxygen on TiO_2 surfaces and found the chemisorbed oxygen to be present on the surface in the form of O^{2-} ions with an accompanying charge transfer from the underlying substrate.

Based on this evidence the following reaction steps are employed in the overall process: Ti is oxidized at the precursor/product interface (R 1). The electrons are transported outward and react with oxygen in a chemisorption step at the product/gas interface (R 2). The reduced oxygen species at the product gas interface reacts with an oxygen vacancy in the titanium dioxide lattice to yield the oxide (R 3). The following reaction mechanism results from this description:

$$\text{at } r = R_i(t): \quad \text{R 1:} \quad \mathrm{Ti} \rightleftharpoons \mathrm{TiO_2} + 2V^{2+} + 4e^- \tag{1}$$

$$\text{at } r = R_o(t): \quad \text{R 2:} \quad S + \frac{1}{2}\mathrm{O_2} + 2e^- \rightleftharpoons SO^{2-} \tag{2}$$

$$\text{R 3:} \quad SO^{2-} + V^{2+} \rightleftharpoons \cdot + S \tag{3}$$

overall:

$$\text{R 1} + 2\,\text{R 2} + 2\,\text{R 3:} \quad \mathrm{Ti} + \mathrm{O_2} \rightleftharpoons \mathrm{TiO_2}. \tag{4}$$

The oxygen vacancy concentration is defined as the difference between the actual concentration of oxygen ions and the stoichiometric concentration of oxygen ions in the lattice (Kubaschewski and Hopkins, 1962):

$$C_V = C_{ox,\text{stoich}} - C_{ox}. \tag{5}$$

From the definition it is clear that while negative oxygen ions will be transported in the direction of the precursor/product interface, the corresponding positive oxygen vacancies (V^{2+}) will be transported outward to the product/gas interface where they will react with adsorbed oxygen (R 3). The $\cdot$ shown in Eq. 3 represents a unit of stoichiometric oxide formed by the reaction of an adsorbed oxygen ion (SO^{2-}) with an oxygen vacancy in the oxide lattice.

S represents the number of unoccupied sites for the chemisorption of oxygen. The total number of sites per unit area, S_T, is fixed (Kubaschewski and Hopkins, 1962) and is the sum of the occupied and unoccupied surface sites:

$$S_T = S + SO^{2-}. \tag{6}$$

Ritchie and Hunt (1969) showed that no qualitative differences should be observed regardless of whether a single site, double site, or more complex oxygen adsorption mechanism is employed, hence the adsorption mechanism described in R 2 is employed. It is convenient to adopt the vacancy formulation (Eqs. 1, 3, and 5), but this does not affect the overall reaction. Summation of R 1, 2× R 2, and 2× R 3 recovers the overall oxidation of titanium to titanium dioxide.

The oxidation process for a metallic particle begins when it is exposed to an oxidizing environment. Oxygen is adsorbed on the surface and reacts to form an initial monolayer of oxide. Due to a chemical potential difference between the metal/oxide and oxide/oxidizer interfaces electrons (e^-) and oxygen vacancies (V^{2+}) are released at the metal/oxide interface by the reaction R 1 as shown in Figure 2. These charges are transported through the oxide layer via a diffusion mechanism driven by concentration gradients. The transport coefficients of ionic species and electrons differ by several orders of magnitude (cf. Tuller, 1981). As the charged species are transported through the product film, separation of charge occurs due to the disparity in transport coefficients. Thus, a self-induced electric field is set up across the product film. This field enhances the slower ionic transport, but adversely affects the faster electron transport so that ultimately the ions and electrons are transported at equivalent rates despite the differences in the magnitude of the respective transport coefficients. It should be stressed that the reactions that occur at the boundaries (R 1, R 2, and R 3) conserve charge, and the overall charge neutrality of the particle is not affected. The potential difference over the product layer is of the order of 1 V (Cabrera and Mott, 1949), but because the product film is initially so thin a very large electric field is generated. Orr (1962) showed that the first monolayer of oxide forms by a process of nucleation and oxide growth at preferred sites on the metal surface. Therefore, the thinnest layer for which a continuum approach could hold would be a monolayer of oxide, or about 5 Å (Fromhold, 1976) and we assume that at least such a monolayer is initially present. Regarding the transport mechanism of electrons in very thin films, Fromhold (1976) suggested that when the films thickness is below 20 Å, quantum mechanical phenomena such as electron tunneling should be considered. Phenomena like electron tunneling and thermal electron emission, important in the initial stages of the overall process, are neglected. The overall reaction process consists of the intraparticle transport of ions and electrons, reaction of these charge species at the precursor/product and product/gas interfaces, and interparticle transport of the gaseous oxidizer. In this article we consider only the intraparticle aspects of the process. Such an approach is correct provided a realistic value is used for the oxygen pressure at the particle surface as can be calculated (Glassman and Law, 1991). The metal is assumed in its highest oxidation state and no recombination effects are considered in the oxide layer. The Einstein relation (Fromhold, 1976) is used to relate the mobility and diffusivity for a given species. The kinetics for the reactions described in Eqs. 1, 2, and 3 are assumed first order with respect to each reactant, and an Arrhenius temperature dependence is assumed. The model does not account for melting, and the process will only be followed below the melting point of the metal. The particle is nonadiabatic and can exchange energy with its surroundings. The particle is assumed spherical with angular symmetry. Thus, only radial dependence will be considered. Analysis of time and space scales (Fromhold, 1976; Rode et al., 1992) showed that when the process is followed on the scale of the changes in the interfaces with respect to time, the species transport, heat conduction, and stresses are at a pseudo-steady state, that is, the steady-state equations can be solved at each point in time as the reaction front moves through the particle.

Governing equations

Fromhold (1963a, 1964, 1976) pioneered the "coupled-currents" approach to this class of reactions, so called because it consistently takes into account the transport of the different charged species. This approach has been increasingly used recently, for example, by Fromm (1989) for metal oxidation, Kapila and Plawsky (1993) who used it to fit solid-state diffu-

sion data in waveguide systems very accurately, and by Rode et al. (1992) to describe the initiation of the combustion of metallic powders.

The oxygen vacancy and electron balances in the product layer are

$$0 = \frac{1}{r^2}\frac{d}{dr}(r^2 J_V) \tag{7}$$

$$0 = \frac{1}{r^2}\frac{d}{dr}(r^2 J_e), \tag{8}$$

where

$$J_V = -D_V\frac{dC_V}{dr} + \mu_V C_V E \tag{9}$$

$$J_e = -D_e\frac{dC_e}{dr} - \mu_e C_e E. \tag{10}$$

The electric field is described by the Poisson equation

$$\frac{1}{r^2}\frac{d}{dr}(r^2 E) = \frac{4\pi e N_A}{\epsilon}(2C_V - C_e). \tag{11}$$

The energy balance in the precursor core and the product shell becomes

$$\frac{d}{dt}[(m_{TiO_2}Cp_{TiO_2} + m_{Ti}Cp_{Ti})T] = 4\pi R_o^2(t)[(-\Delta H)J_V - h(T - T_{amb})], \tag{12}$$

where

$$\frac{dm_{Ti}}{dt} = -4\pi R_i^2(t) M_{Ti}\,\mathrm{R}\,1 \tag{13}$$

$$\frac{dm_{TiO_2}}{dt} = -4\pi R_i^2(t) M_{TiO_2}\,\mathrm{R}\,1. \tag{14}$$

Surface reactions

A single reaction takes place at the metal/oxide interface, $r = R_i(t)$. R 1 is defined in terms of TiO_2, and from Eq. 1 we obtain

$$\mathrm{R}\,1 = k_1\tilde{C}_{Ti} - k_{-1}\tilde{C}_V\tilde{C}_e, \tag{15}$$

where the $\tilde{C}$'s represent surface concentrations and are calculated as suggested by Fromhold (1976).

Two reactions take place at the oxide/gas interface, $r = R_o(t)$. Oxygen is adsorbed through a charge transfer reaction and the adsorbed oxygen takes the place of an oxygen vacancy in the lattice to form an entity of stoichiometric oxide (indicated by a $\cdot$), thus liberating a free site at the surface. Both R 2 and R 3 are defined in terms of SO^{2-}, and we obtain from Eqs. 2 and 3:

$$\mathrm{R}\,2 = k_2\tilde{C}_S P_{O2}\tilde{C}_e - k_{-2}\tilde{C}_{SO^{2-}} \tag{16}$$

$$\mathrm{R}\,3 = k_3\tilde{C}_{SO^{2-}} - \tilde{C}_V - k_{-3}\tilde{C}_S. \tag{17}$$

Boundary conditions

The boundary conditions for the electron and anion vacancy balances are specified in terms of the reactions. Since there is no accumulation on the interface, the net flux of each species entering the interface is equal to the rate of consumption of that species:

$$\left.\begin{aligned} J_V &= 2\,\mathrm{R}\,1 \\ J_e &= 4\,\mathrm{R}\,1 \end{aligned}\right\} \quad \text{at} \quad r = R_i(t), \tag{18}$$

$$\left.\begin{aligned} J_V &= \mathrm{R}\,3 \\ J_e &= 2\,\mathrm{R}\,2 \end{aligned}\right\} \quad \text{at} \quad r = R_o(t). \tag{19}$$

The boundary condition for the Poisson equation can be formulated for either of the two boundaries, for example, at $R_o(t)$ (Fromhold, 1976):

$$E = -\frac{4\pi e N_A}{\epsilon}\left(2\tilde{C}_V - \tilde{C}_e - 2\tilde{C}_{SO^{2-}}\right). \tag{20}$$

$\tilde{C}_{SO^{2-}}$, which is the surface concentration of adsorbed oxygen ions and exists only at the product/gas interface, that is, at $R_o(t)$, can be calculated from the statement that $J_e = 2J_V$ at $R_o(t)$:

$$\tilde{C}_{SO^{2-}} = \frac{\tilde{C}_T\left(k_2 P_{O_2}\tilde{C}_e + k_{-3}\right)}{k_2 P_{O_2}\tilde{C}_e + k_{-2} + k_3\tilde{C}_V + k_{-3}}. \tag{21}$$

The mobility for the electrons was obtained from Göpel et al. (1983). The parameter values used are shown in Table 1.

Numerical Method

The initial state of the system is uniquely described by the temperature, pressure, and geometric description of a powder particle. Solution of the transport equations and the Poisson equation (Eqs. 7 to 11) yields the electric and concentration fields and provides the reaction rate. Temperature changes in the particle are given by the solution of the lumped energy balance (Eq. 12). The stress distributions in the precursor core and product shell as well as the changes in the interface radii, $R_i(t)$ and $R_o(t)$, are given by solution of the

Table 1. Transport Properties for Anion Vacancies and Electrons

Property	Unit
$D_V = 10e^{-126{,}000/RT}$	m^2/s
$\mu_e = 10^2 T^{-2.5}$	$m^2/V/s$

stress equations. The reader is referred to recent work by Rode et al. (1994) for a detailed description of the stress equations and the corresponding numerical method. Thus, these three sets of equations—the transport, energy balance, and mechanical stress equations—have to be solved simultaneously.

Given the temperature, pressure, and geometric description of the powder particle, the transport equations are solved. The reaction rate thus calculated is used to update the time, energy balance, and stress formulation (stress distributions including the interface radii).

The system is nonlinear and of the convection/diffusion/reaction type, with the convection term dominating. It is well known that this type of degenerated diffusion equation represents a serious numerical problem. Two of us accumulated important information on the solution of this type of problem in the area of plasma enhanced CVD (Orlicki et al., 1992). The shooting method (Finlayson, 1980) is a simple method to solve this system; however, extreme values of the Peclet number usually prevent effective application of this method unless some modification is applied.

Due to the fact that the chemical reactions enter only as boundary conditions, flux is conserved in the domain. This serves as an invariant and allows for simplification of the system, that is, reduction of two second-order equations and a first-order equation to three first-order equations. Consequently two, rather than four boundary conditions are needed for an initial estimate. The procedure is indicated for the oxygen vacancy balance (Eq. 7). Integrating Eq. 7 from $R_o(t)$ to arbitrary r we obtain:

$$r^2 J_V = R_o^2(t) J_V \mid_{R_o(t)}. \tag{22}$$

Applying this procedure to the electron balance as well (Eq. 8), inserting the expressions for the oxygen vacancy and electron fluxes (Eqs. 9 and 10), and carrying out the differentiation in the Poisson equation (Eq. 11), the following system of three first-order differential equations is obtained:

$$\frac{dC_V}{dr} = \frac{\mu_V}{D_V} C_V E - \left[\frac{R_o^2(t)}{r^2}\right] J_V \mid_{R_o(t)} \tag{23}$$

$$\frac{dC_e}{dr} = -\frac{\mu_e}{D_e} C_e E - \left[\frac{R_o^2(t)}{r^2}\right] J_e \mid_{R_o(t)} \tag{24}$$

$$\frac{dE}{dr} = -\frac{2E}{r} + \frac{4\pi e N_A}{\epsilon}(2C_V - C_e). \tag{25}$$

If the values of $\tilde{C}_V$ and $\tilde{C}_e$ at $R_o(t)$ are known, integration of Eqs. 23 to 25 can be carried out.

Solution of the transport equations thus entails finding the set of $(\tilde{C}_V \mid_{R_o(t)}, \tilde{C}_e \mid_{R_o(t)})$, which satisfies the governing equations and the boundary conditions. After initial guesses for $\tilde{C}_V \mid_{R_o(t)}$ and $\tilde{C}_e \mid_{R_o(t)}$ are made, these values are updated by using a Newton scheme with a numerical Jacobian based on the satisfaction of the following two criteria:

$$\left[2\,\mathrm{R}\,1\left(\tilde{C}_{V,\mathrm{calc}}, \tilde{C}_{e,\mathrm{calc}}\right) R(t)\right] \mid_{R_i(t)} - \left[\mathrm{R}\,3\left(\tilde{C}_V, \tilde{C}_e\right) R(t)\right] \mid_{R_o(t)} = 0, \tag{26}$$

which ensures that flux is conserved, and also that

$$\left[E_{\mathrm{calc}} - \frac{4\pi e N_a}{\epsilon}\left(2\tilde{C}_{V,\mathrm{calc}} - \tilde{C}_{e,\mathrm{calc}}\right)\right] \mid_{R_i(t)} = 0, \tag{27}$$

which ensures charge neutrality. $E_{\mathrm{calc}} \mid_{R_i(t)}$, $\tilde{C}_{V,\mathrm{calc}} \mid_{R_i(t)}$, and $\tilde{C}_{e,\mathrm{calc}} \mid_{R_i(t)}$ are evaluated in the following manner, given $\tilde{C}_V \mid_{R_o(t)}$ and $\tilde{C}_e \mid_{R_o(t)}$:

1. Calculate $\tilde{C}_{SO^{2-}}$ from Eq. 21. This ensures that R 2 = R 3, that is, that the electron and anion vacancy fluxes are equivalent. Now calculate $J_V \mid_{R_o(t)}$ and $J_e \mid R_o(t)$.
2. Determine E at $R_o(t)$ from the boundary condition for the Poisson equation stated at $R_o(t)$ (Eq. 20).
3. Back integrate Eq. 23 to 25 from $R_o(t)$ to $R_i(t)$ using the Runge–Kutta method. This yields E_{calc}, $\tilde{C}_{V,\mathrm{calc}}$, and $\tilde{C}_{e,\mathrm{calc}}$ at $R_i(t)$.

Back integration was followed here because it gives lower sensitivity to the initial guess, but forward integration is also possible with a slight change in the iteration procedure (Marek and Hlavacek, 1966). The calculation was initiated with a low Peclet number combined with continuation because the equations are parametrically sensitive and an inappropriate initial guess results in a numerical explosion.

Results and Discussion

The anion vacancy, electron, and electric field profiles are shown in Figure 3 for different product layer thicknesses of 20, 50, 100 and 200 Å for a particle size of 10μm and at 300 K. Consider the anion vacancy concentration profiles shown in Figure 3a, which have been expressed as a deviation from the stoichiometric composition of TiO_2. A deviation of 0.5% corresponds to a stoichiometric formula of $TiO_{1.99}$ whereas 0.05% corresponds to $TiO_{1.999}$. The vacancy concentration is highly dependent on the thickness: for a very small product layer thickness, relatively large nonstoichiometry is observed, but at the ultimate thickness of 100 to 200 Å the degree of nonstoichiometry at room temperature is very small. This trend is consistent with experimental evidence that relatively few defects are observed at low temperature. The electron concentration profiles are shown in Figure 3b. The electron concentration exhibits an opposite trend compared to the anion vacancy concentration: whereas the anion vacancy concentration decreases as the product layer thickness increases, the electron concentration increases. This trend is due to the fact that the anion vacancies and electrons have opposite charge. A positive electric field is self-induced across the product layer during the course of the reaction process. This field aids transport of vacancies but inhibits transport of the electrons. Therefore, as the product layer thickness increases (and also the diffusion resistance), the electric field has to decrease (cf. Figure 3c). In order for the system to decrease the positive electric field, the vacancy concentration decreases while the electron concentration increases. This trend is borne out by the decrease in the magnitude of the electric field shown in Figure 3c as the product layer thickness increases. It should be emphasized that the system regulates the magnitude of the electric field, and the charge neutrality of the particle is not affected—the excess positive charge in the product layer is matched exactly by the negative charge

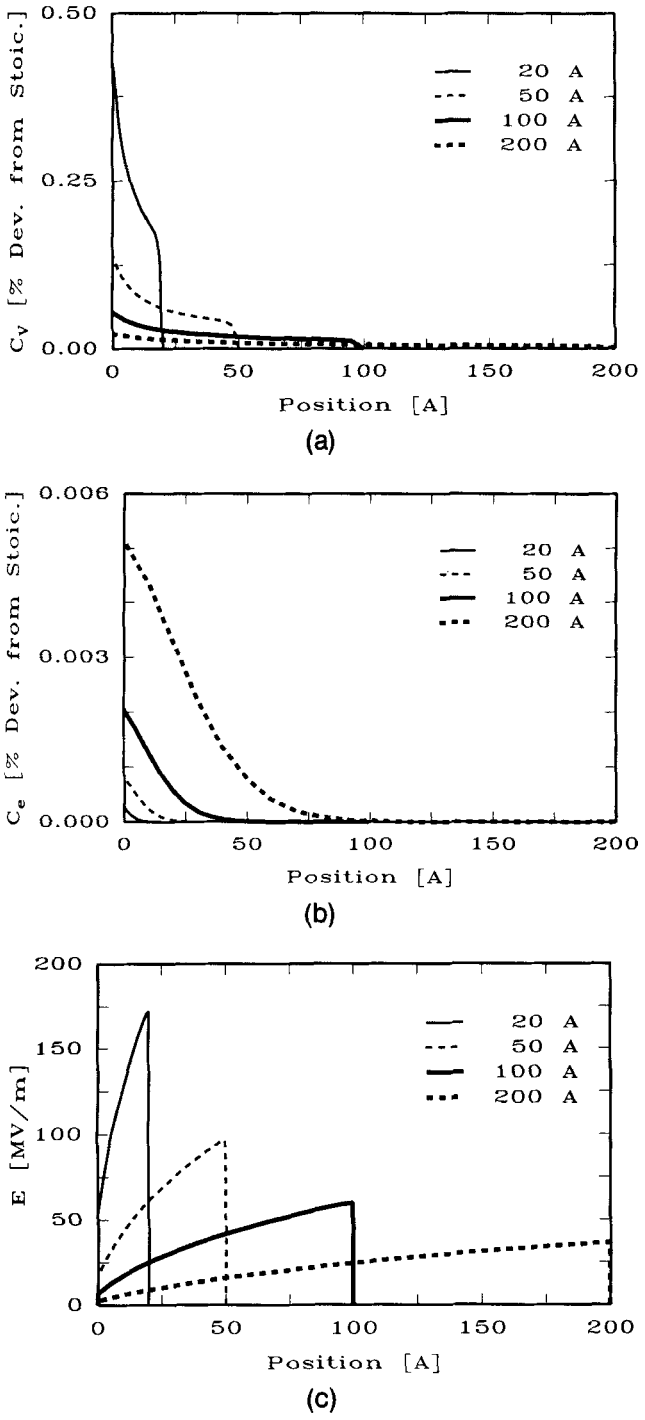

Figure 3. Profiles at different product layer thicknesses of 20, 50, 100 and 200 Å.

(a) Anion vacancy concentration profiles. (b) Electron concentration profiles. (c) Electric field profiles.

on the product/gas interface as demonstrated conceptually in Figure 2. This is the cause for the discontinuity in the electric field at the product/gas interface, where the positive electric field that is formed within the product layer is canceled exactly by the negatively charged oxygen ions adsorbed on the surface. Thus, the electric field is generated to balance the anion vacancy and electron fluxes to ensure charge neutrality even though the transport coefficients of the vacancies and electrons differ by many orders of magnitude.

The increase of the product layer thickness is plotted against time in Figure 4 for a particle size of 10 μm and at 300 K. The solid line shows the actual increase in thickness due to transport by diffusion caused by the concentration gradients shown in Figures 3a and 3b and convection caused by the electric field demonstrated in Figure 3c. The dashed line shows the growth rate when the mobility of the oxygen vacancies is set to zero, in which case the vacancy transport is caused by diffusion only. This provides a method to quantify the relative contribution of the two transport mechanisms. In general the diffusion coefficient and mobility of oxygen anions are related by the Einstein relation, so that this case would correspond to a different mechanism where an uncharged species, for example, atomic oxygen, diffuses through the product layer. It is clear from Figure 4 that the convective transport mechanism, caused by the large electric field, is at least as important as the traditional diffusion mechanism. Whenever the transport coefficients of the different charged species, oxygen vacancies, and electrons in this case, differ significantly, charge separation will occur in the product layer and an electric field will be formed across the product layer. This electric field, which enhances the transport of species with lower transport coefficients and inhibits the transport of species with higher transport coefficients, is the key to maintaining overall charge neutrality.

The overall reaction rate shown in Figure 4 is initially very rapid, but then declines dramatically. This point is emphasized by the observation that as the product layer thickness increases 20 times, the reaction rate decreases 750 times. The shape of the growth curve is approximately logarithmic, which is in agreement with experimental evidence on Ti oxidation (Kubaschewski and Hopkins, 1962) even though no logarithmic dependence is included in the governing equations or boundary conditions. This is due to the interaction of the electric field with the transport process. The resistivity of the material calculated from the total current density of anion vacancies and electrons using the method suggested by Shackelford (1992) of 5×10^{10} to 1×10^{12} Ωm is in good

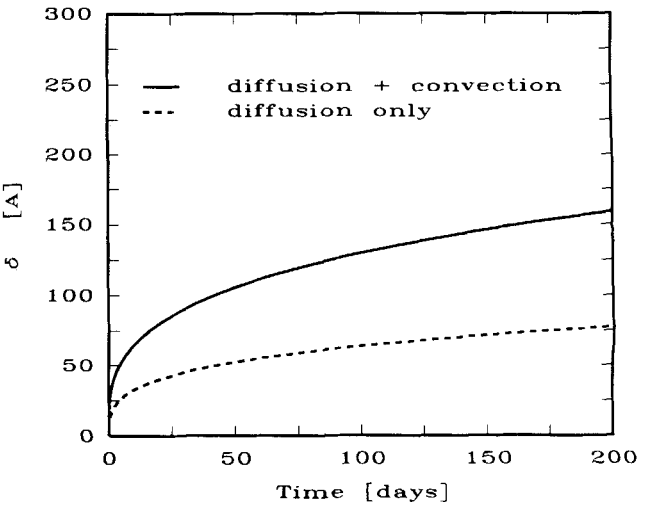

Figure 4. Thickness of the oxide layer vs. time for a 10-μm particle.

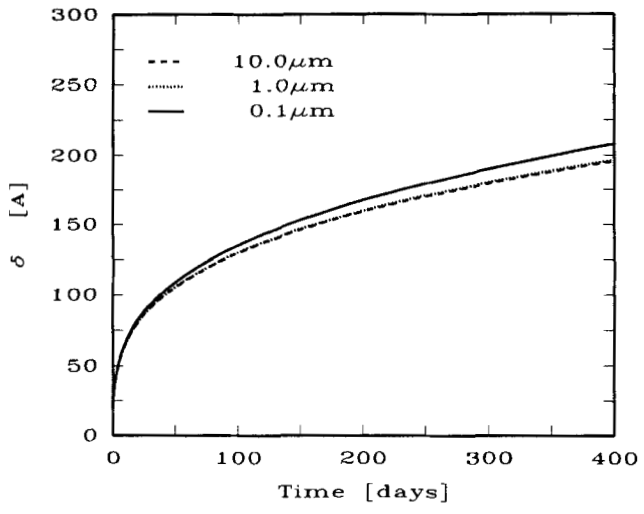

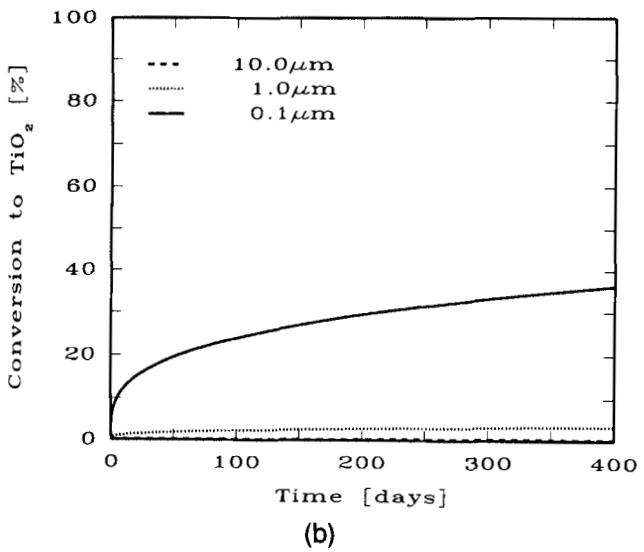

Figure 5. Influence of particle size.

(a) Thickness of the oxide layer vs. time. (b) Conversion to TiO_2 vs. time.

agreement with the resistivity values reported by Pampuch (1988) of 10^{11} to 10^{12} Ωm for rutile ceramics.

The influence of particle size on the product layer thickness and conversion is shown in Figure 5. In Figure 5a the thickness of the product layer is only slightly larger for the 1-μm particle than for the 10-μm particle. Due, however, to the spherical geometry, the product layer thickness starts to become significantly larger for the 0.1-μm particle as time proceeds. Of course, for a given product layer thickness the conversion is inversely proportional to the particle size, as shown in Figure 5b and after a given amount of time the finest particle is much further converted to oxide than the 1- and 10-μm particles. This point emphasizes a major problem with fine powders—even small product layer thicknesses correspond to significant levels of contamination, degrading the desired properties of the material significantly. This higher conversion attributable to finer powders also plays a major part in determining the stress behavior.

The influence of particle size on the evolution of pressure within a particle is shown in Figure 6. The total pressure at any point within a particle has been defined as the first-order invariant:

$$\Gamma(r) = \frac{1}{3}[\sigma_{rr}(r) + \sigma_{\theta\theta} + \sigma_{\phi\phi}(r)]. \tag{28}$$

It was found that the total pressure was the highest at the product/gas interface, hence this position is represented in Figure 6. As discussed, the product layer thicknesses are similar for all three particle sizes. However, the conversions differ significantly (Figure 5b). The stress and hence the pressure is dependent on the conversion. Therefore, the pressure increases with decreasing particle size. As shown in Figure 6a, the pressure in the 10-μm particle is most likely too small to cause mechanical degradation of the film. In the case of

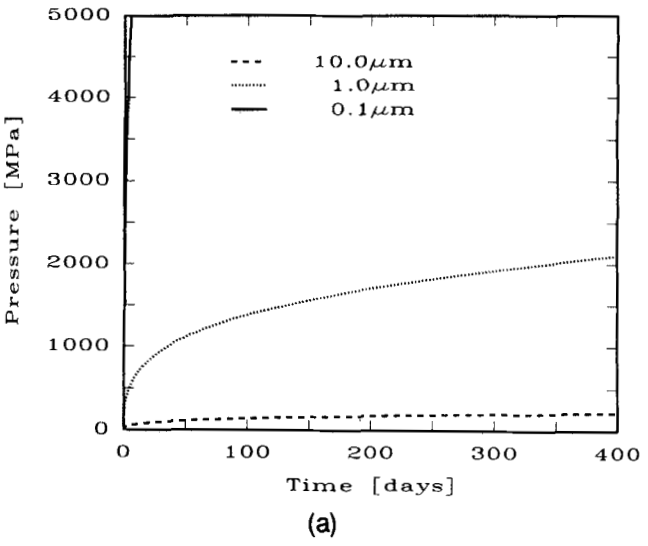

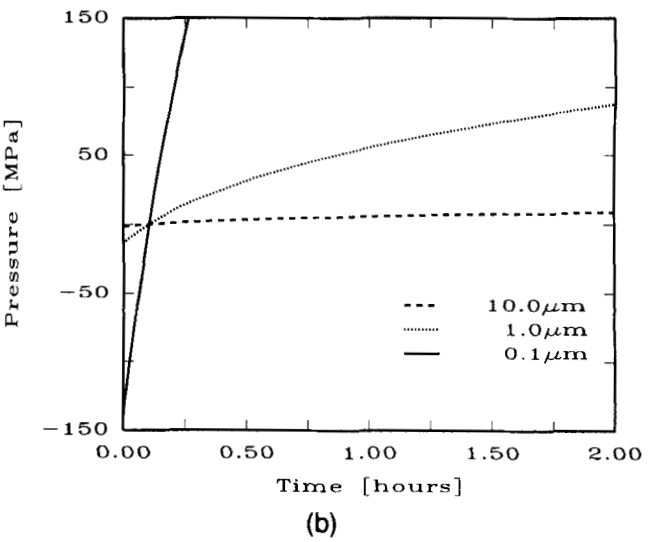

Figure 6. Influence of particle size on total pressure within the particle at the product/gas interface.

(a) Total pressure vs. time. (b) Initial total pressure vs. time.

the 1-μm particle the pressure exceeds the strength of the material and mechanical degradation of the product film is possible. In the case of the 0.1-μm particle the pressure exceeds the strength of the material by such an extent that stress relaxation, most probably through mechanical degradation, would occur. Even though the mechanical stresses would not degrade the product layer of the 10-μm particle at room temperature, at higher temperatures of a few hundred degrees, the Arrhenius temperature dependence of the reaction process dictates that much thicker product layers will form. This will increase the conversion significantly and could cause the 10-μm particle to degrade mechanically, as has indeed been observed by Rode et al. (1994).

If the stress in a particle exceeds the strength of the material, mechanical degradation occurs. This manifests in three measurable ways: (1) the surface area increases significantly, (2) spalling can be observed by SEM, and (3) the contaminant concentration in the powder (usually oxygen) increases greatly. Experimental evidence has been provided by Rode et al. (1994). In a very interesting study Sakka et al. (1992) considered the oxidation and degradation of ultrafine titanium nitride powders exposed to air. This study by Sakka et al. (1992) is somewhat analogous to the study conducted by Rode and Hlavacek (1994), who studied Ti powder of about 10-μm particle size, but for a much smaller particle size of about 0.02 μm. Sakka et al. (1992) found that the ultrafine powders degraded when exposed to air for periods varying from 3 months to 5 years—even at room temperature. They found that the oxygen content increased rapidly and in addition the surface area increased greatly, from 32 to 102 m^2/g. This result is in agreement with Figure 6a. Rode et al. (1994) found that the surface area of Ti powder increases up to seven times when mechanical degradation occurred.

Another interesting aspect of the pressure is shown in Figure 6b where the pressure evolution of the initial 2 h of exposure to oxygen is plotted. The initial monolayers of product are formed under a negative pressure, whereas subsequent layers are formed under a positive pressure. This is caused by the effect of surface energy that tends to compress the particle. As discussed in Rode et al. (1994), the contribution of the surface energy is extremely particle-size-dependent and, for a particle size of 1 μm and below, cannot be neglected. The observation that the initial monolayers of product film will be formed under conditions of negative pressure has important implications on the properties of the film, which would differ dramatically from product layers that are formed subsequently under conditions of positive pressure. This result also demonstrates why very fine materials react differently from larger bodies with lower curvature.

The stress profiles after 1 year are shown in Figures 7 and 8 for the 1-μm and 0.1-μm particle, respectively. The radial stresses are compressive everywhere while the tangential stresses are compressive in the precursor core and tensile in the product layer. The role played by surface energy in the stress behavior of fine powders was discussed in detail by Rode et al. (1994) and is demonstrated in Figures 7 and 8. Consider Figure 7a, which shows the radial stresses in a 10-μm particle. The effect of surface energy is inversely proportional to the particle radius and is responsible for the discontinuity at the metal/oxide interface as well as the fact that the radial stress equals the sum of atmospheric pressure and

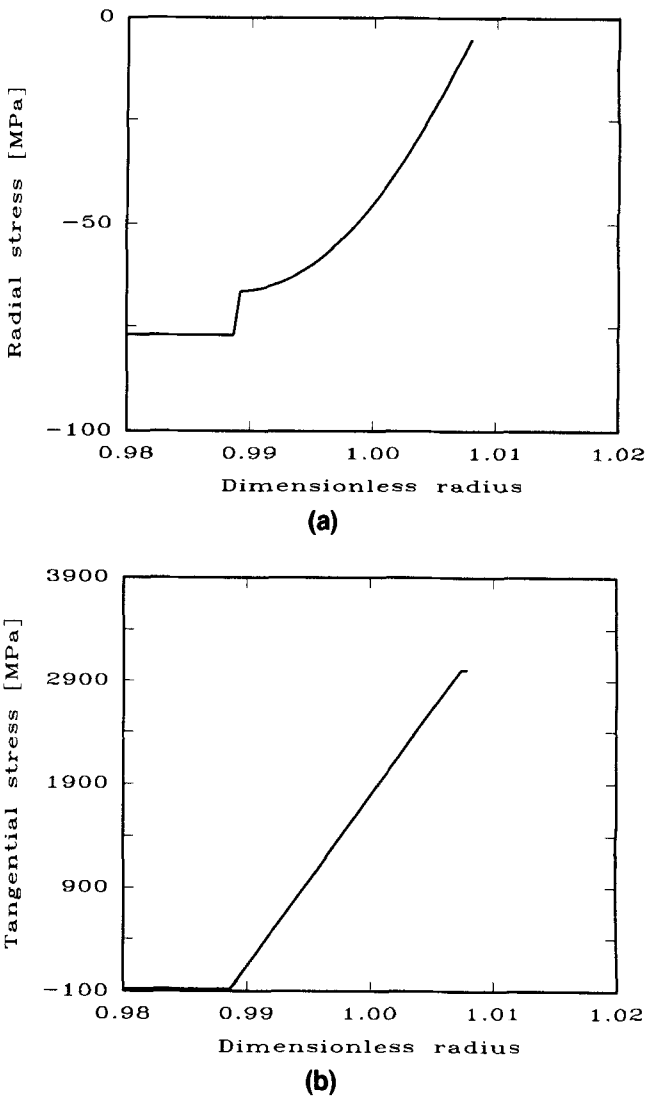

Figure 7. Stress profiles for a 1-μm particle after 1 year.

(a) σ_{rr} vs. dimensionless radius. (b) $\sigma_{\theta\theta}$ vs. dimensionless radius.

a contribution of the surface energy at the oxide/gas interface (cf. Rode et al., 1994). The tensile tangential stresses in the product layer are very large, especially in the case of the 0.1-μm particle and it is most probable that mechanical degradation would occur in this case. In reality the stresses may be considerably smaller than presented in this study: bulk properties were used; however, there is evidence, as discussed by Rode et al. (1994) that these product films may have significantly different properties compared to bulk materials, for example, a significantly smaller elastic modulus, which would lead to much lower stresses.

Another feature of Figures 7 and 8 is the evidence of swelling as a function of conversion: the 1-μm particle, which has undergone a 3.3% conversion (cf. Figure 5b), has swollen to the extent of a 0.8% increase in the outer radius; the 0.1-μm particle that has been converted to 35% has swollen to the extent of a 7% increase in radius. This swelling of the particle as the reaction front propagates throughout the sam-

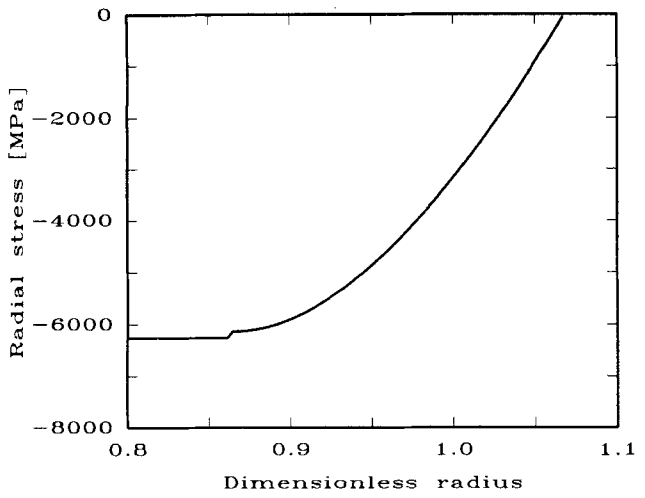

(a)

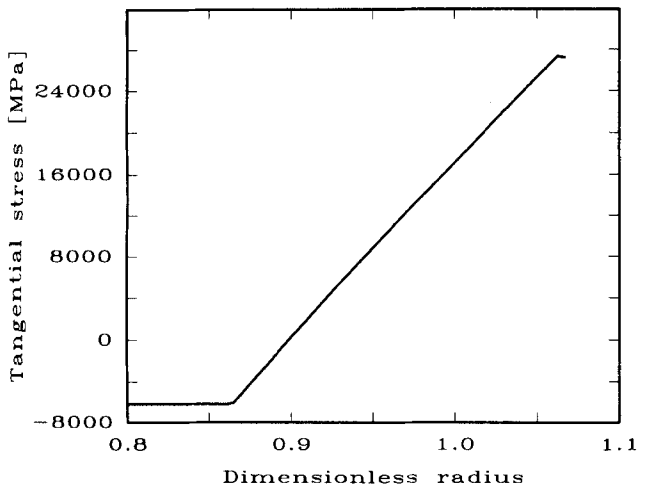

(b)

Figure 8. Stress profiles for a 0.1-μm particle after 1 year.

(a) σ_{rr} vs. dimensionless radius. (b) $\sigma_{\theta\theta}$ vs. dimensionless radius.

ple is well known. Szekely et al. (1976) realized that the increase in volume would affect the reaction kinetics by increasing the product layer thickness through which the limiting reactant has to diffuse (cf. Figure 1). Recently, Pigeon and Varma (1993) incorporated this important aspect into their determination of the single-particle kinetics of silicon nitridation. These studies, which take the change in volume —and ensuing change in diffusion resistance—into account, are certainly valid. However, the major impact that this volume change has on the mechanical stress distribution in the particle has been largely disregarded. The stresses created during the course of the reaction become extremely large, of the order of the strength of the material and larger and will affect the kinetics quantitatively and qualitatively by leading to mechanical degradation of the film.

The results presented in this article certainly provide a high degree of consistency and detail, although certain experimentally observed phenomena are not matched. This does not represent a failure of the model, but rather a choice to limit the complexity for this initial study. Perhaps of more importance than these differences, is the fact that this model can be systematically extended to include aspects that are currently lacking. It is therefore interesting to discuss some of the elements not incorporated by the present model.

It has been observed for fine powders that suboxides tend to form as well. Averback et al. (1989) synthesized a black, nanocrystalline titanium dioxide corresponding to the stoichiometric formula $TiO_{1.7}$. Rode et al. (1994) oxidized coarser powders and observed violet and blue phases, most probably corresponding to Ti_2O_3 and Ti_3O_5. Transport and stress generation will be different in these suboxides. Most notably, these suboxides have lower Pilling–Bedworth ratios, which will lead to lower stresses during oxidation. In this study the assumption was made that the only product phase is nonstoichiometric titanium dioxide. Large deviations from stoichiometry and the resulting formation of Magnéli phases, which are two phase regions (cf. Reed, 1970), and suboxides, were not modeled.

We can speculate that the large space charge that is generated during the oxidation process influences not only the rate of oxidation, as demonstrated in this study (cf. Figure 4), but also the extent of the reaction, that is, the formation of suboxides. Ikeda and Chiang (1993) have shown that there is an interaction between the defect structure and the space charge for titanium dioxide.

Furthermore, properties were considered independent of the electric and stress fields. Yet these fields are very large and a further interaction should exist, as demonstrated by the following two examples for related problems. Electrostriction, the phenomenon where a stress field is generated when an electric field is applied across a dielectric, has been shown by Nelson and Oriani (1992) to be of importance in oxide systems. The diffusion process should also depend on the stresses present in the system as discussed by Chu and Lee (1990) for elastic two-phase media. Such couplings should be addressed in future contributions.

A key to including these aspects is the adoption of an extended description of the Gibbs free energy, which would also include the stress components as mechanical variables. The foundation for such an approach has been discussed by Li (1978). An additional obstacle in the extension of this work will be to obtain reliable properties for some of the suboxides such as Ti_2O_3 and Ti_3O_5 as well as highly nonstoichiometric titanium dioxide.

Summary and Conclusions

This article built upon the foundation developed by Rode et al. (1994), where it was identified that mechanical stresses play an important role in the overall reaction kinetics of gas–solid systems in general. The need was identified to develop a consistent model that simultaneously involves the species transport processes and the generation of mechanical stresses. Such a model was developed for the case study of titanium oxidation. The description of species transport includes diffusion due to concentration gradients as well as convection due to a self-induced electric field caused by charge separation. The charge separation is a function of disparate transport coefficients, a feature that is widely exhibited by oxide, nitride, and sulfide systems. Convection was

found to be at least as important as diffusion for the system studied. This result should also apply to many other systems.

The transport and stress processes are inherently coupled as shown in this development and it is not possible to integrate the system in time without simultaneously solving the transport and stress equations unless significant simplification is introduced.

The results also show that certain experimentally observed phenomena are not matched by the present model. Future work, which will include the formation of substoichiometric phases and the coupling of the electric field, stress, and transport properties, may elucidate some of these aspects better.

Notation

C = volumetric concentration, kmol/m^3
C_p = heat capacity, J/kg/K
D = diffusivity, m^2/s
E = electric field, V/m
e^- = electron
e = charge of electron, C
$(-\Delta H)$ = heat of reaction, J/kmol
h = heat-transfer coefficient, J/m^2/s/K
J = flux, kmol/m^2/s
k = reaction constant, varies
m = mass of solid, kg
M = molecular weight, kg/kmol
N_A = Avogadro number, no./kmol
$\mathbf{P}$ = solid product
R = radial boundary, m
r = radial coordinate, m
S = surface, m^2
t = time, s
T = temperature, K
V^{2+} = oxygen vacancy, kmol/m^3

Greek letters

ϵ = permittivity, C/V/m
μ = mobility, m^2/V/s
θ = angular coordinate
ρ = density, kg/m^3
σ = stress, Pa
ϕ = angular coordinate

Subscripts

amb = ambient
e = electron
i = precursor/product interface
ox = oxide
o = product/gas interface
ref = reference
s = surrounding
V = oxygen vacancy

Literature Cited

Averback, R. S., H. Hahn, H. J. Höfler, J. L. Logas, and T. C. Shen, "Kinetic and Thermodynamic Properties of Nanocrystalline Materials," Vol. 153, B. M. DeKoven, A. J. Gellman, and R. Rosenberg, eds., *Interfaces Between Polymers, Metals and Ceramics*, Materials Res. Society, Pittsburgh, p. 3 (1989).

Buessem, W. R., and S. R. Butler, "Defect Reactions in TiO_2," *Kinetics of High-Temperature Processes*, W. D. Kingery, ed., Wiley, New York, p. 13 (1959).

Cabrera, N., and N. F. Mott, "Theory of the Oxidation of Metals," *Progr. Phys. Rep.*, **12**, 163 (1949).

Chu, J. L., and S. Lee, "Diffusion-Induced Stresses in Two-Phase Elastic Media," *Int. J. Eng. Sci.*, **28**, 1085 (1990).

Colson, J. C., M. Lambertin, and P. Barret, "The Formation Process of Central Cavities during Growth of Thick Layers of Metallic Sulphur," *Reactivity of Solids*, J. S. Anderson, M. W. Roberts, and F. S. Stone, eds., Chapman & Hall, London, p. 283 (1972).

Finlayson, B. A., *Nonlinear Analysis in Chemical Engineering*, McGraw-Hill, New York (1980).

Fromhold, A. T., "Kinetics of Oxide Film Growth on Metal Crystals: I" *J. Phys. Chem. Solids*, **24**, 1081 (1963a).

Fromhold, A. T., "Kinetics of Oxide Film Growth on Metal Crystals: II," *J. Phys. Chem. Solids*, **24**, 1309 (1963b).

Fromhold, A. T., "Kinetics of Oxide Film Growth on Metal Crystals: III. Perturbation Treatment of Space Charge Fields," *J. Phys. Chem. Solids*, **25**, 1129 (1964).

Fromhold, A. T., *Theory of Metal Oxidation*, North-Holland, Amsterdam (1976).

Fromm, E., "Model Calculations of Metal Oxidation at Ambient Temperatures," *Non-Stoichiometric Compounds, Surfaces, Grain Boundaries and Structural Defects*, J. Nowotny and W. Weppner, eds., Kluwer, New York, p. 523 (1989).

Glassman, I., and C. K. Law, "Sensitivity of Metal Reactivity to Gaseous Impurities in Oxygen Environments," *Combust. Sci. Tech.*, **80**, 151 (1991).

Göpel, W., G. Rocker and R. Geierabend, "Intrinsic Defects of TiO_2 (110): Interaction with Chemisorbed O_2, H_2, CO, and CO_2," *Phys. Rev. B*, **28**, 3427 (1983).

Heinrich, V. E., G. Dresselhaus, and J. J. Zeiger, "Chemisorbed Phases of O_2 on TiO_2 and $SrTiO_3$," *J. Vac. Sci. Technol.*, **15**, 534 (1978).

Ikeda, J. A. S., and Y.-M. Chiang, "Space Charge Segregation at Grain Boundaries in Titanium Dioxide: I, Relationship between Lattice Defect Chemistry and Space Charge Potential," *J. Amer. Ceram. Soc.*, **76**, 2437 (1993).

Ishida, M., and C. Y. Wen, "Comparison of Kinetic and Diffusional Models for Solid-Gas Reactions," *AIChE J.*, **14**, 311 (1968).

Kapila, D., and J. L. Plawsky, "Solid-State Film Diffusion for the Production of Integrated Optical Waveguides," *AIChE J.*, **39**, 1186 (1993).

Kofstad, P., "Thermogravimetric Studies of the Defect Structure of Rutile (TiO_2)," *J. Phys. Chem. Solids*, **23**, 1579 (1962).

Kofstad, P., "Note on the Defect Structure of Rutile (TiO_2)," *J. Less-Common Metals*, **13**, 635 (1967).

Kofstad, P., *Nonstoichiometry, Diffusion, and Electrical Conductivity in Binary Metal Oxides*, Wiley, New York (1972).

Kubaschewski, O., and B. E. Hopkins, *Oxidation of Metals and Alloys*, 2nd ed., Butterworths, London (1962).

Levenspiel, O., *Chemical Reaction Engineering*, 2nd ed., Wiley, New York (1972).

Li, J. C.-M., "Physical Chemistry of Some Microstructural Phenomena," *Metall. Trans. A*, **9A**, 1353 (1978).

Marek, M., and V. Hlavacek, "Axialer Stoff-und Wärmetransport im Adiabatischen Rohrreaktor: I. Gleichungen und Lösungsmethoden," *Chem. Eng. Sci.*, **21**, 493 (1966).

Munnix, S., and M. Schmeits, "Origin of Defect States on the Surface of TiO_2," *Phys. Rev. B*, **31**, 3369 (1985).

Nelson, J. C., and R. A. Oriani, "Stress Generation during Anodic Oxidation of Titanium and Aluminum," *Corros. Sci.*, **34**, 307 (1992).

Orlicki, D., V. Hlavacek, and H. J. Viljoen, "Comparison of Different Ionization Models for a Glow Discharge," *AIChE J.*, **38**, 1835 (1992).

Orr, W. H., "Oxide Nucleation and Growth," PhD Diss., Cornell Univ., Ithaca, NY (1962).

Pampuch, R., *Constitution and Properties of Ceramic Materials*, Elsevier, New York (1988).

Park, J. Y., and O. Levenspiel, "The Crackling Core Model for the Reaction of Solid Particles," *Chem. Eng. Sci.*, **30**, 1207 (1975).

Pigeon, R. G., and A. Varma, "Quantitative Kinetic Analysis of Silicon Nitridation," *J. Mater. Sci.*, **28**, 2999 (1993).

Pilling, N. B., and R. E. Bedworth, "The Oxidation of Metals at High Temperatures," *J. Inst. Metals*, **29**, 529 (1923).

Reed, T. B., "The Role of Oxygen Pressure in the Control and Measurement of Composition in 3d Metal Oxides," *The Chemistry of Extended Defects in Non-Metallic Solids*, L. Eyring, and M. O'Keeffe, eds., North-Holland, Amsterdam, p. 21 (1970).

Ritchie, I. M., and G. L. Hunt, "The Kinetics and Pressure Dependence of Surface Controlled Metal Oxidation Reactions," *Surf. Sci.*, **15**, 524 (1969).

Rode, H., and V. Hlavacek, "An Experimental Study of Titanium Powder Reactivity in Gaseous Environments: I. Oxidation," *Comb. Sci. Technol.*, **99**, 143 (1994).

Rode, H., "Modeling of Reactivity, Reaction Rate Evaluation and Experimental Strategy in Non-Catalytic Gas-Solid Reactions," PhD Diss., State Univ. of New York at Buffalo (1994).

Rode, H., D. Orlicki, and V. Hlavacek, "Reaction Rate and Mechanical Stress in Gas-Solid Systems: Experimental Evidence and Theoretical Analysis," *AIChE J.*, **41**, 1235 (1995).

Rode, H., H. J. Viljoen, J. E. Gatica and V. Hlavacek, "Combustion of Metallic Powders: A Phenomenological Model for the Initiation of Combustion," *Combust. Sci. Tech.*, **88**, 153 (1992).

Sakka, Y., S. Ohno, and M. Uda, "Oxidation and Degradation of Titanium Nitride Ultra Fine Powders Exposed to Air," *J. Amer. Ceram. Soc.*, **75**, 244 (1992).

Shackelford, J. F., *Introduction to Materials Science for Engineers*, 3rd ed., Macmillan, New York (1992).

Sohn, H. Y., and J. Szekely, "A Structural Model for Gas-Solid Reactions with a Moving Boundary: III. A General Dimensionless Representation of the Irreversible Reaction between a Porous Solid and a Reactant Gas," *Chem. Eng. Sci.*, **27**, 763 (1972).

Szekely, J., J. W. Evans, and H. Y. Sohn, *Gas-Solid Reactions*, Academic Press, New York (1976).

Tuller, H. L., "Mixed Conduction in Nonstoichiometric Oxides," *Nonstoichiometric Oxides*, O. T. Sorenson, ed., Academic Press, New York, p. 271 (1981).

Wagner, C., "Beitrag zur Theorie des Anlaufvorgaugs," *Z. Phys. Chem. B*, **21**, 25 (1993).

Zhong, Q., J. M. Vohs, and D. A. Bonnell, "Local Structure and Defects on Hydrogen- and Vacuum Reduced TiO_2 Surfaces," *J. Amer. Ceram. Soc.*, **76**, 1137 (1993).

Manuscript received Aug. 19, 1994, and revision received Jan. 11, 1995.